Artical ID:1006-3471(2012)06-0537-11

Kinetic Study of Photoelectrochemical Oxidation of Lignin Model Compounds on TiO_2 Nanotubes

Min Tian, Daniel Liba, Aicheng Chen*

(*Department of Chemistry, Lakehead University, 955 Oliver Road, Thunder Bay, Ontario P7B 5E1, Canada*)

Abstract: In this study, TiO_2 nanotubes were prepared via the electrochemical oxidation of titanium substrates in a non-aqueous electrolyte and their morphology and microstructures were examined by scanning electron microscopy (SEM) and X-ray diffraction (XRD). The photoelectrochemical oxidation of two lignin model compounds, 1-(3,4-dimethoxyphenoxy)-2-(2-methoxyphenoxy)-1,3-propanediol (DMP) and 3-hydroxy-1-(3,4-dimethoxyphenoxy)-2-(2-methoxyphenoxy)-1,3-propanone (HDM), was investigated. A new band appeared at ~ 304 nm during the photoelectrochemical oxidation of DMP. The rate of DMP intermediate formation was amplified with the increase of initial concentrations, while it was diminished with increased temperature. Despite the similarity in structure between HDM and DMP, there are only small increases in absorbance during the oxidation of HDM, suggesting that HDM is less reactive. Quantum chemical calculations based on the density functional theory (DFT) were performed in order to link photoelectrochemical reactivity with specific molecular properties. Relatively higher E_{LUMO}-E_{HOMO} of HDM makes it more stable and thus more refractory to oxidation, which is consistent with our photoelectrochemical results.

Key words: photoelectrochemical oxidation; TiO_2 nanotubes; UV-Vis spectroscopy; lignin model compounds; DFT calculation

CLC Number: O646 **Document Code:** A

1 Introduction

Lignin, a tridimensional amorphous phenolic polymer comprised of phenylpropane units linked together by various bonds, is the major byproduct of the pulp and paper industry[1]. After being separated from the cellulosic mass, in most cases lignin is either combusted in energy and caustic recovery boilers, as is the practice in many Kraft mills, or it makes its way into waste streams, which adversely impacts river and lake systems. Various treatment methods such as electrochemical oxidation[2-4], activated electrosorption[5], chemical oxidation, and biological digestion[6] have been investigated for the modification[7-8] or degradation[9] of organic compounds, including lignin[10], in aqueous systems.

Heterogeneous photocatalysis[11-12] is a promising alternative technique for the elimination of organic pollutants from wastewater[13-15]. Among the various oxide semiconductor photocatalysts, titania (TiO_2) is one of the most promising because of its biological and chemical inertness, cost effectiveness, and robust oxidizing power via the prevalence of photogenerated holes[16-17]. TiO_2 has three natural phases, namely, brookite, anatase, and rutile. Of these phases, anatase is typically considered to be the most active[18]. When TiO_2 is present in the form of a slurry/suspension, the photochemical reaction is

Received: 2012-06-18, Revised: 2012-07-31 *Corresponding author, Tel: 1-807-3438318, E-mail: aicheng.chen@lakeheadu.ca
This work was supported by a Strategic Grant from the Natural Sciences and Engineering Research Council of Canada (NSERC). A. Chen acknowledges NSERC and the Canada Foundation of Innovation (CFI) for the Canada Research Chair Award in Materials and Environmental Chemistry.

enhanced due to the large available surface area/volume ratio. However, there are two significant problems associated with this approach: (i) TiO_2 must be recovered from the treated water, which is a challenge for large scale applications; and (ii) The efficiency is low due to the recombination of the electron-hole pairs.

Supported semiconductors can provide an alternative solution to the separation problem. However, photocatalysis through the use of thin films also has a number of disadvantages when compared with powders. Firstly, the surface area that is available for exposure to the liquid phase is reduced by 2 ~ 3 orders of magnitude. Secondly, the diffusion boundary conditions are altered from binary collisions to that of particles that are adhered to a substrate, wherein the mass transfer may become the limiting step. Thus, a high surface area to volume ratio[19-20] (e.g., nanoscale TiO_2[21-22]) is desirable for improving the efficacy of photocatalysis using thin films.

Lignin is a complex polymer that is constructed of phenylpropane monomers, which are linked primarily through C—O ether bonds, and to a lesser extent, through various C—C alkyl-aryl and di-aryl bonds. The dominant C—O ether linkages are β-Aryl (β-O-4), α-Aryl (α-O-4) and diphenyl (4-O-5) types. The inherent complexity of the lignin polymer makes it difficult to evaluate in terms of reaction kinetics. Consequently, relatively simple molecules that contain isolated functional groups or typical lignin bonding patterns can be utilized to reveal detailed information of mechanistic processes. According to the primary chemical structure of lignin, as briefly stated above, and the previous studies[23-25], in this study, we chose the following two lignin model compounds: 3-hydroxy-1-(3,4-dimethoxyphenoxy)-2-(2-methoxyphenoxy)-1,3-propanone (HDM) and 1-(3,4-dimethoxyphenoxy)-2-(2-methoxyphenoxy)-1,3-propanediol (DMP). The structures of the two model compounds used in the present work are shown in Fig. 1. UV-Vis spectroscopy was employed to monitor the time-dependent concentration changes during the photoelectrochemical oxidation of the lignin model compounds (DMP and HDM), aiming to provide some mechanistic insights of the photoelectrochemical oxidation of lignin. The directly observable absorbance/concentration changes provide an effective approach for the kinetic analysis.

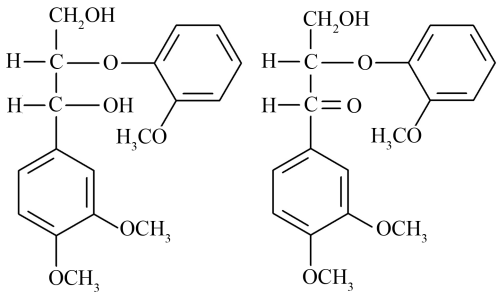

Fig. 1 Structure of 1-(3,4-dimethoxyphenoxy)-2-(2-methoxyphenoxy)-1,3-propanediol (DMP) and 3-hydroxy-1-(3,4-dimethoxyphenoxy)-2-(2-methoxyphenoxy)-1,3-propanone (HDM).

2 Experimental

2.1 Materials

DMP and HDM were synthesized according to an established procedure[24], All other chemicals were of reagent grade and were used as supplied. The water (18.2 MΩ·cm) for the preparation of all solutions was purified by a Nanopure Diamond® water system. Stock solutions were made by dissolving the DMP and HDM in a 0.1 mol·L^{-1} NaOH solution. Subsequent concentrations were obtained by diluting the stock solution with a 0.1 mol·L^{-1} NaOH solution.

2.2 Preparation and Characterization of TiO_2 Nanotube

Pure Ti substrates were degreased by sonication in acetone for 10 min and then in the pure water for an additional 10 min. The Ti substrates were then etched in 18% hydrochloric acid at 85°C for 15 min. The etched titanium plate was rinsed thoroughly with pure water, followed by anodization in dimethyl sulfoxide (DMSO) with 2% HF at 40 V for

8 h [13]. After the electrochemical treatment, the samples were rinsed thoroughly with pure water and dried in an argon stream. In order to obtain a defined anatase structure, the samples were annealed for one hour at 450 °C. The crystalline structure and phase of the TiO_2 nanotubes were examined using an X-ray diffraction (XRD, Philips PW 1050-3710 diffractometer with Cu K_α radiation), and the morphology was characterized by scanning electron microscopy (SEM, JEOL JSM 5900LV). Gas chromatography/mass spectrometry (GC/MS, Varian 450/300) was used to identify the intermediates that were generated in the course of the photoelectrochemical process.

2.3 Photoelectrochemical Experiment

An EG&G 2273 potentiostat/galvanostat was used to apply an anodic potential bias during the photo-degradation of the DMP and HDM. TiO_2 nanotubes were synthesized and used as the working electrode in this study. The counter electrode consisted of a Pt coil. Prior to each experiment the counter electrode was cleaned by flame annealing and then quenched with pure water. The reference electrode was an Ag/AgCl electrode. The solution in the cell was under continuous mixing using a small magnetic stirrer bar. An ADAC Systems™ Cure Spot™ 50 UV spot lamp (main line of emission - 365 nm) was utilized for the irradiation of the TiO_2 nanotubes. The intensity of the UV light was ca. 2 $mW \cdot cm^{-2}$. The UV light was introduced into the cell via a fiber optic cable, which was placed above the electrode. The distance between the UV-visible light and the electrode surface was 1 cm. The absorbance measurements were carried out by means of a computer controlled Cary 50 UV-vis spectrometer.

2.4 Quantum Chemical Calculation

DFT (Density Functional Theory) methods were carried out using Gaussian 03, a quantum-mechanical program, for molecular modeling. The calculation was based on the B3LYP method[26] and 6-31*G basis set[27] at ambient temperature. This basis set provided accurate geometry and electronic properties for a wide range of organic compounds. The DFT/B3LYP method defines the exchange functional as a linear combination of Hartree-Fock, local, and the gradient-corrected exchange terms. This exchange functional is then combined with a local and/or gradient-corrected correlation functional of Lee, Yang and Parr (LYP). All quantum theoretical calculations were carried out with full geometry optimizations. The following quantum chemical descriptors were calculated: the energy of the highest occupied molecular orbital (E_{HOMO}), the energy of the lowest unoccupied molecular orbital (E_{LUMO}), and the dipole moment (μ).

3 Results and Discussion

3.1 Characterization of TiO_2 Nanotubes

Fig. 2 depicts SEM images of TiO_2 nanotube arrays that were synthesized by the electrochemical oxidation of titanium substrates at 40 V for 8 h in a non-aqueous electrolyte (DMSO/HF). From the SEM images, it is evident that the self-organized nanotubes with lengths of ca. 2 μm, form regular arrays with pores that have uniform diameters of ca. 60 nm. It is also clear that the pore mouths are open at the top of the layer while the nanotubes are closed at the bottom of the layer. The length and diameter of TiO_2 nanotubes can be affected by both the type of solvent and the amount of HF. The enhanced length of the TiO_2 nanotubes that were grown in organic solvent might be attributed to the presence of less water, which decreases the solubility of TiO_2.

Anatase is known to be the most efficient TiO_2 structure for photocatalysis. In previous work we confirmed that anatase TiO_2 provides a high decomposition rate for salicyclic acid[15]. Thus, the TiO_2 nanotube electrodes were annealed at 450 °C in order to convert them to an anatase structure. The resulting structure of the prepared TiO_2 nanotubes was confirmed by diffraction peaks in the XRD pattern presented in Fig. 2B. It is evident that the peak at $2\theta = 25.4°$ is the crystal of the tetragonal anatase TiO_2 phase. The peaks marked with an asterisk are derived from the Ti substrate.

3.2 Photochemical and Photoelectrochemical Oxidation of DMP in Alkaline

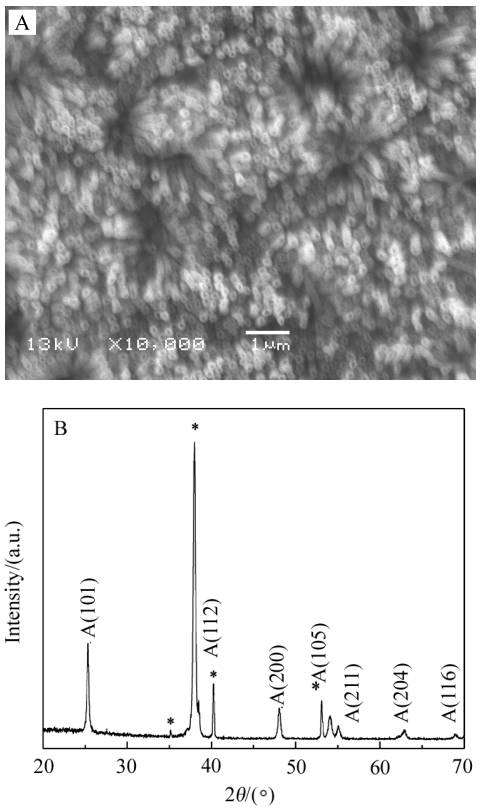

Fig. 2 SEM image (A) and XRD pattern (B) of the titanium oxide nanotubes prepared at 40 V for 8 h in DMSO+ 2% HF.

The photochemical and photoelectrochemical oxidation of DMP were carried out at the TiO_2 nan otubes in a 0.1 mol·L^{-1} NaOH solution, and monitored by UV-Vis spectroscopy. Fig. 3A shows the spectral absorbance of 100 μg·mL^{-1} DMP in 0.1 mol· L^{-1} NaOH taken at two-minute intervals during 40 min of photochemical oxidation and at ten-minute intervals for the remaining time. It was observed that the absorbance at the range spanning 240 ~ 400 nm increased with time, indicating that intermediates were produced in the course of the photochemical oxidation of DMP. The absorbance reached its maximum after 40 min, after which it began to decrease, as shown in the inset of Fig. 3A. This demonstrates that the intermediates may also be photochemicalally oxidized. The color of the solution changed to yellow after 40 min upon UV irradiation and became colorless subsequent to 5 h irradiation. The band at ca. 276 nm was blue-shifted to 266 nm, and its height decreased to 1.87 after ca. 3 h (curve a in Fig. 3C), corresponding to a 40% oxidation of DMP.

Fig. 3B shows a plot of the photoelectrochemical oxidation of DMP at TiO_2 nanotubes in a 0.1 mol·L^{-1} NaOH solution. The applied potential was 0.6 V vs. Ag/AgCl. A 0.6 V applied potential did not, without UV, result in any oxidation of DMP. A new band appears again for DMP at ca. 304 nm and reaches the maximum at ca. 20 min. This indicates the formation of intermediates during the process of photoelectrochemical degradation of DMP. Subsequent to increasing to their maximum at 275 nm and 304 nm, absorbance began to decrease and approached to 0.25 at 275 nm (curve b in Fig. 3C), corresponding to 85% removal of the DMP. There are two significant changes that are apparent in the absorption spectra depicted in Fig. 3B. One is the amount of time that is required to attain the maximum (20 min rather than 40 min) for the formation of intermediates. The second is the enhanced degradation of DMP; the efficiencies of DMP degradation in 3 h are 40% and 85% for photochemical and photoelectrochemical oxidation, respectively. The higher efficiency of the photoelectrocatalytic process may be attributed to the suppression of the recombination of photogenerated holes and electrons.

It is known that photocatalysts are first excited by UV light, which subsequently initiates the photochemical process. TiO_2 nanotubes absorb light and generate electron/hole pairs (Eq. 1).

$$TiO_2 + h\nu \rightarrow TiO_2(e_{cb}^- + h_{vb}^+) \quad (1)$$

Since the position of the TiO_2 valence band is high, the photogenerated holes can oxidize a wide variety of organic substrates.

$$TiO_2(h^+) + S \rightarrow TiO_2 + S^+ \quad (2)$$

In order to improve the efficiency of the oxidation process, the recombination of the photogenerated charge carriers must be avoided. This may be accomplished by applying an external potential bias [28-29]. It was assumed that the small size of the TiO_2 particles resulted in only a very weak electric field[30], which

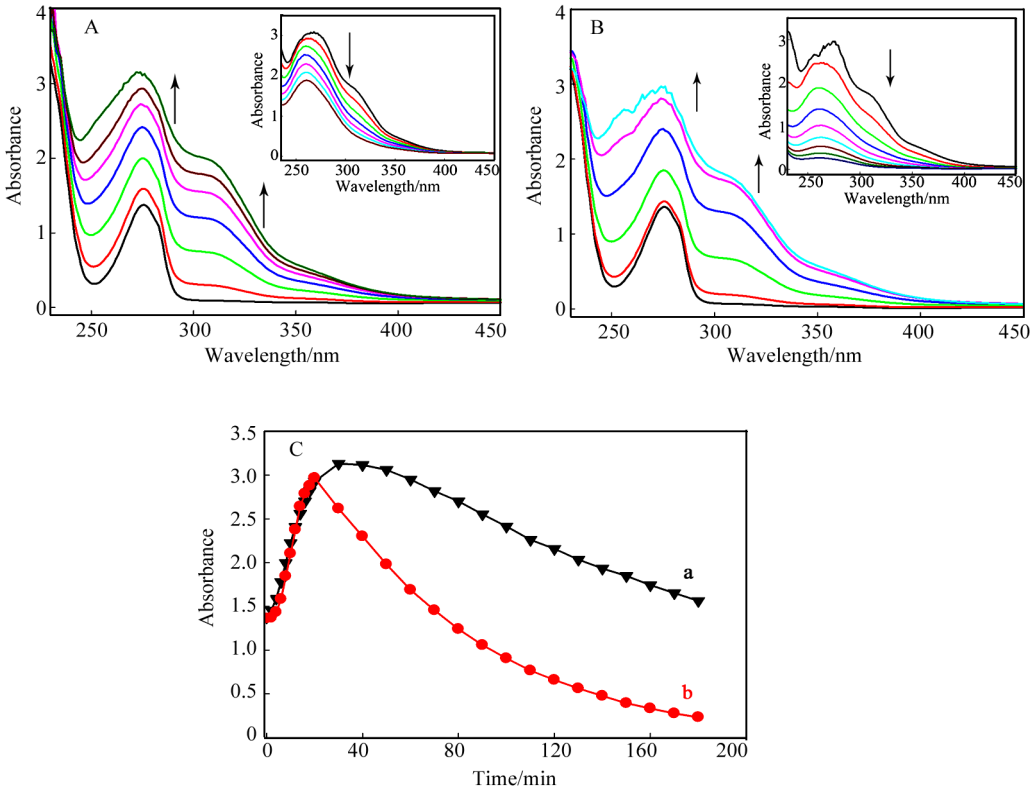

Fig. 3　Photochemical (A), photoelectrochemical (B) oxidation of 100 μg·L^{-1} DMP in 0.1 mol·L^{-1} NaOH, and the plot of absorbance vs. time during photochemical (a) and photoelectrochemical (b) oxidation of DMP (C) (insets show the oxidation of intermediates, applied potential/V: 0.6, arrows show the direction of progression of the curves).

was insufficient to facilitate charge separation. The high degradation rates obtained through the application of a potential to the TiO_2 electrode was attributed to increased charge separation efficiencies driven by the differing rates of electron and hole transfer at the solution interface.

To identify the byproducts that were generated by the lignin model compounds, the solution was acidified to pH 1 ~ 2 with HCl following 20 min of photochemical and photoelectrocatalytic oxidation. The intermediates were extracted with CH_2Cl_2, which was subsequently dehydrated with anhydrous Na_2SO_4 and analyzed using GC/MS. 3,4-dimethoxybenzaldehyde was identified as the primary intermediate with *m/z* 166.

3.3 Photoelectrochemical Oxidation of HDM in Alkaline

Fig. 4 shows the spectral absorbance of 100 μg·mL^{-1} HDM in 0.1 mol·L^{-1} NaOH taken at two-minute intervals during 40 min of photochemical oxidation, and at ten-minute intervals for the remaining time. Absorbance at 280 nm increases with the irradiation time in 20 min (Fig. 4A), and then starts to decrease (Fig. 4B) for the remaining time. It is readily seen that a new peak appeared at ca. 260 nm during the HDM oxidation process. Interestingly, there is no increase at ca. 304 nm and the increase at 280 nm is much slower than that of DMP despite the similarity in structure between HDM and DMP (Fig. 1).

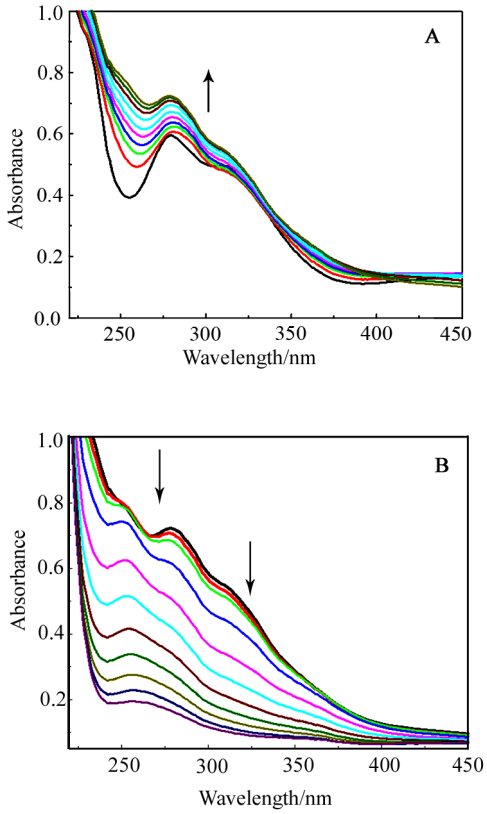

Fig. 4　Photoelectrochemical oxidation of 100 μg·mL^{-1} HDM (A) and intermediates (B) in 0.1 mol·L^{-1} NaOH (applied potential/V: 0.6, arrows show the direction of the progression of the curves).

The above experimental results show that the photochemical oxidation of DMP and HDM may proceed via different reactive pathways. More intermediates were formed from DMP after a short irradiation time, suggesting that a non-phenolic lignin model DMP compound with a-hydroxyl groups should be more reactive. The photochemical oxidation of DMP may proceed via the cleavage of the arylglycerol ether structure[31], rather than the oxidation of the α-hydroxyl group to C═O. This is an important factor insofar as the light-induced yellowing of high-yield pulps. However, further work is required to evaluate the mechanism of the photochemical processes.

3.4 Kinetics of Photoelectrochemical Oxidation of DMP

It is well known that the photoelectroehemical oxidation of most organic compounds can be analyzed using the Langmuir-Hinshelwood model[32-33].

$$-\frac{dC}{dt} = k_r \frac{k_a C}{1+k_a C} \quad (3)$$

where $-(dC/dt)$ is the photochemical oxidation rate, k is the photochemical oxidation rate constant, k_a is the adsorption equilibrium constant, and t is the reaction time. If the product of k_a and C is significantly smaller than 1, the above equation can be simplified to a first-order reaction:

$$-\frac{dC}{dt} = k_r k_a C \quad (4)$$

Consequently an integrated form of eq. (2) can be represented as follows:

$$\ln\left(\frac{C_o}{C}\right) = k_{app} t \quad (5)$$

where $k_{app} = k_r k_a$ is the apparent rate constant in min^{-1}. The k_{app} value can be obtained by plotting ln (C_o/C) versus t.

Fig. 5 presents the absorbance vs. time for the formation (A) and disappearance (B) of intermediates during the photoelectrochemical oxidation of various initial concentrations of DMP in 0.1 mol·L^{-1} NaOH. The concentration was varied and spanned the range of 25 to 100 μg·mL^{-1}. It can be clearly seen that the formation of intermediates is dependent on the initial concentration of DMP. There are additional intermediates formed as the initial concentration of DMP increases. The absorbance of intermediates at 304 nm is ca. 1.86 at an initial concentration of 100 μg·mL^{-1}, which is an order of magnitude larger than that of 25 μg·mL^{-1}. Similar behavior was observed at 276 nm. It is interesting to note that the shape of the curves is contingent on the initial concentration as well. The S-shape was observed at an initial concentration of 100 μg·mL^{-1}, while a nearly linear relationship between absorbance and time was obtained at 25 μg·mL^{-1}.

Typical scanning-kinetics plots obtained at 304 nm as a function of irradiation time are shown in Fig. 5B. These simulations, based on first order kinetics, give the solid line in Fig. 5B, and are consistent with the experimental data. First order kinetics

was also confirmed by the linear relationship of ln (C/C_0) versus irradiation time (eq. 5), giving a first order rate constant value of k_{app} = 0.010, 0.011 and 0.012 min^{-1} for 100, 75 and 50 μg·mL^{-1}, respectively, showing that the rate constants are almost independent of the initial concentrations of DMP.

3.5 Effect of Temperature

We further investigated the kinetics of the photoelectrochemical oxidation of HDM and DMP at various temperatures, which were controlled by a Fisher thermostat. Fig. 6A and 6B presents the spectral absorbance during the photoelectrochemcal oxidation of 100 μg·mL^{-1} DMP at 10 and 50 °C, respectively. The absorption band at 304 nm increased with time at both temperatures, as observed in Fig. 3B. It is worth noting that the band at 275 nm increased at a much slower rate at 50 ℃ (Fig. 6B), indicating that a low temperature favors the formation of the intermediate. Fig. 7 displays the plots of the absorbance at 280 nm vs. time for the photoelectrochemic al oxidation of HDM at different temperatures, showing that the increase of the temperature decreased the time for the formation and further degradation of the intermediate.

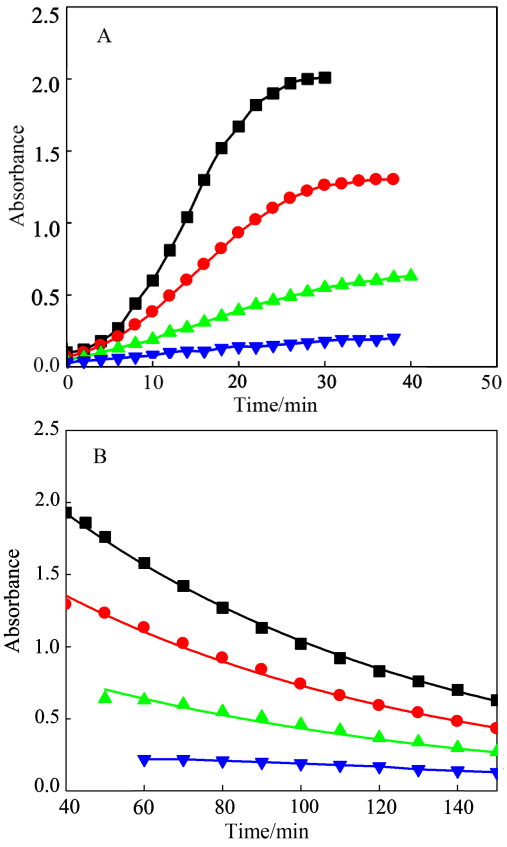

Fig. 5 Absorbance vs. time plots for the formation (A) and disappearance (B) of intermediates during photoelectrochemical oxidation of various initial concentrations of DMP in 0.1 mol·L^{-1} NaOH.
DMP concentration: (■) 100 μg·mL^{-1}, (●) 75 μg·mL^{-1}, (▲) 50 μg·mL^{-1}, (▼) 25 μg·mL^{-1}

It is found experimentally for many reactions that a plot of lnk_{app} against 1/T gives a straight line. This behavior is normally expressed mathematically by Arrhenius equation:

$$\ln k_{app} = \ln A - E_a/RT \quad (6)$$

where parameter A, which corresponds to the intercept of the line at $1/T = 0$, is called the pre-exponen tial factor. The parameter E_a, which is obtained from the slope of line, represents activation energy. Generally speaking, the higher the activation energy, the stronger the temperature dependence of the rate constant.

The Arrheninus plots based on the kinetics data

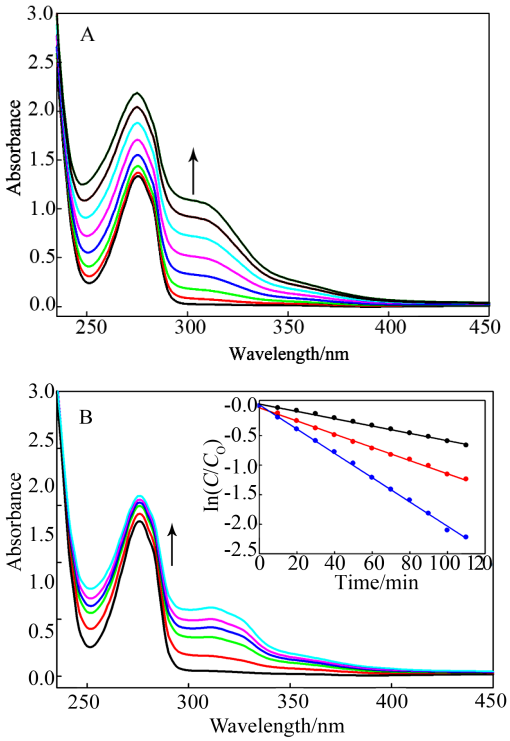

Fig. 6 Scanning kinetics data for the photoelectrochemical oxidation of 100 μg·mL^{-1} of DMP at 10 ℃ (A) and 50 ℃ (B) (the inset shows ln(C/C_0)-t curves at various temperatures).

(insets in Fig. 6B and Fig. 7) determined at 20, 40 and 60 ℃ yield two straight lines, from which the apparent activation energy was estimated to be 21.8 and 24.6 kJ·mol^{-1} for the photoelectrochemical oxidation of the intermediates resulted from HDM and DMP, respectively. These values are quite close to those of hydroxyl radical reactions, suggesting that the photoelectrochemical oxidation process is governed by the hydroxyl radical reaction[34-35].

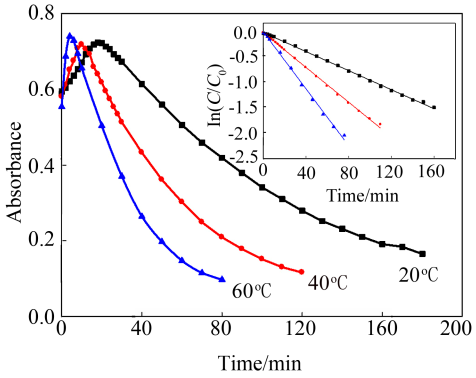

Fig. 7 Absorbance vs. time curves for the photoelectrochemical oxidation of 100 μg·mL^{-1} of HDM in 0.1 mol·L^{-1} NaOH (the inset shows ln (C/C_0)-t curves with various temperatures).

3.6 Quantum Chemical Study of HDM and DMP

Quantum chemical calculations were performed in order to correlate the order of the photoelectrochemical reactivity of HDM and DMP with electron structure. Quantum chemistry calculations have been successfully applied to study of reaction mechanisms [36], to solve chemical reaction ambiguities, as well as to correlate chemical reactivity with molecular orbital (MO) energy. It has been reported that the E_{HOMO} is often associated with the electron donating ability of the molecule. High E_{HOMO} values indicate a tendency a molecule to donate electrons to acceptor molecules that have a low energy orbital arrangement. Similarly, E_{LUMO} represents the ability of a molecule to accept electrons. Lower E_{LUMO} values suggest that a molecule will accept electrons more easily, whereas the highest occupied molecular orbital-lowest unoccupied molecular orbital energy ΔE(energy gap) serves as a simple measure of chemical stability[37-38]. Tab. 1 represents the results of E_{HOMO} (eV), E_{LUMO} (eV), E_L-E_H (eV), μ(Debye) and total relative energy calculated by the B3LYP method in the gas phase for DMP and HDM. It is clearly seen from Tab. 1 that the substitution of C═O in HDM by C—OH results in a decrease in dipole moments, and energy difference ΔE (3.0 eV), respectively. The higher energy gap (ΔE) of HDM makes it more stable[38-39] and thus more resistant to oxidation. This is consistent with our results, which were derived from the photoelectrochemical oxidation of DMP and HDM.

Tab. 1 Molecular properties of DMP and HDM calculated using B3LYB/6-31G

	DMP	HDM
E_{HOMO}/eV	-5.74	-5.91
E_{LUMO}/eV	-4.90	-1.96
ΔE/eV	0.84	3.95
E(total energy/AU)	-1161.52	-1160.93
Dipole moment(D)	3.96	5.73

4 Conclusions

TiO_2 nanotubes were grown directly on a Ti substrate via electrochemical oxidation in a DMSO/HF solution. The photoelectrochemical oxidation of DMP and HDM was investigated at TiO_2 nanotubes in 0.1 mol·L^{-1} NaOH, and the process was monitored using a UV-Vis spectrophotometric method. The results obtained demonstrate that the efficiency of the photochemical oxidation of lignin model compounds can be significantly improved through the application of an external potential bias. In a 100 μg·mL^{-1} solution, 85% of DMP was removed upon three-hour UV irradiation. It is important to note that a new band appeared for DMP at ca. 304 nm, indicating that the intermediates were formed at the onset of the UV irradiation. Our GC/MS results revealed that 3,4-dimethoxyben-

zaldehyde was the primary intermediate, which can be further degraded completely with the increase of the oxidation time. The photoelectrochemical oxidation of both DMP and HDM follows the first-order kinetics. The rate constants are nearly independent of initial concentrations, while strongly dependant on temperature. The higher energy gap (ΔE) of HDM based on the DFT calculation makes it more stable and thus more difficult to oxidize, which is consistent with our results from the photoelectrochemical oxidation of DMP and HDM.

Acknowledgements

This work was supported by a Strategic Grant from the Natural Sciences and Engineering Research Council of Canada (NSERC). A. Chen acknowledges NSERC and the Canada Foundation of Innovation (CFI) for the Canada Research Chair Award in Materials and Environmental Chemistry.

References:

[1] Wu D, Shi Q C, Zhou J T, et al. Deep treatment of pulping wastewater using three phase fluidized bed electrode reactor[J]. Journal of Electrochemistry, 2006, 12(4): 412-415.

[2] Pan K, Tian M, Jiang Z H, et al. Electrochemical oxidation of lignin at lead dioxide nanoparticles photoelectrodeposited on TiO_2 nanotube arrays[J]. Electrochimica Acta, 2012, 60: 147-153.

[3] Tian M, Bakovic L, Chen A. Kinetics of the electrochemical oxidation of 2-nitrophenol and 4-nitrophenol studied by in situ UV spectroscopy and chemometrics[J]. Electrochimica Acta, 2007, 52(23): 6517-6524.

[4] Li T C, Zhu S L. Research on phenol wastewater treatmentbyelectrochemicaloxidation [J]. Journalof Electrochemistry, 2005, 11(1): 101-104.

[5] Wang B C, Sun Y P. Adsorption and oxidation of phenol electrodeprocesses[J]. Journal of Electrochemistry, 2003, 9(4): 475-478.

[6] O'Connor O A, Young L Y. Toxicity and anaerobic biodegradability of substituted phenols under methanogenic conditions[J]. Environmental Toxicology and Chemistry, 1989, 8(10): 853-862.

[7] Tian M, Wen J L, MacDonald D, et al. A novel approach to convert lignin into value-added products [J]. Electrochemistry Communications, 2010, 12(4): 527-530.

[8] Liu Y, Liu D, Zhao S L, et al .Electrochemical oxidation of the phenol in the chloride system[J]. Journal of Electrochemistry, 2007, 13(1): 30-34.

[9] Li Z F. Electrochemical disinfection method to treat wastewater from hospitals[J]. Journal of Electrochemistry, 2005, 11(4): 420-424.

[10] Tolba R, Tian M, Wen J L, et al. Electrochemical oxidation/modification of lignin at IrO_2-based mixed oxide electrodes[J]. Journal of Electroanalytical Chemistry, 2010, 649(1/2): 9-16.

[11] Cao B, Xu J W, Ding L H, et al. Preparation and electrochemical characterization of anatase TiO_2 nanotubes [J]. Journal of Electrochemistry, 2006, 12(4): 445-448.

[12] Lan B B, Zhou J Z, Xi Y Y, et al. Special Photoelectrochemical response of nano-crystalline TiO_2 electrode [J]. Journal of Electrochemistry, 2006, 12(1): 16-19.

[13] Tian M, Thind S S, Chen S, et al. Significant enhancement of the photoelectrochemical activity of TiO_2 nanotubes[J]. Electrochemistry Communications, 2011, 13 (11): 1186-1189.

[14] Egerton T A, Christensen P A, Harrison R W, et al. The effect of UV absorption on the photocatalytic oxidation of 2-nitrophenol and 4-nitrophenol[J]. Jouranal of Applied Electrochemistry, 2005, 35(7/8): 799-813.

[15] Tian M, Adams B, Wen J L, et al. Photoelectrochemical oxidation of salicyclic acid and salicylaldehyde on titanium dioxide nanotube arrays [J]. Electrochimica Acta, 2009, 54(14): 3799-3805.

[16] Yang S M, Wang J C, Kou H Z, et al. Influence of tert-butylpyridine on the band energetics of nanostructured TiO_2 electrodes and the photoelectrochemical properties of dye-sensitized electrodes [J]. Journal of Electrochemistry, 2011, 17(2): 204-211.

[17] Yun H, Lin C J, Li J, et al. Photoelectrochemical properties of N, S, and Cl modified nano TiO_2 thin films[J]. Journal of Electrochemistry, 2010, 16(4): 411-415A.

[18] Zhang Y H, Zhang H X, Xu Y X, et al. Significant effect of lanthanide doping on the texture and properties of nanocrystalline mesoporous TiO_2[J]. Journal of Solid State Chemistry, 2004, 177(10): 3490-3498.

[19] Wu P F, Li M C, Shen J N, et al. Preparation of photo-electrochemical anticorrosion TiO_2 films by anodization method[J]. Journal of Electrochemistry, 2004, 10 (3): 353-358.

[20] Wu G, Wen J, Nigro S, et al. One-step synthesis of N&F co-doped mesoporous TiO_2 photocatalysts with high visible light activity [J].Nanotechnology, 2010, 21: 085701/1-6.

[21] Shibata T, Sakai N, Fukuda K, et al. Photocatalytic properties of titania nanostructured films fabricated from titania nanosheets[J]. Physical Chemistry Chemical Physics, 2007, 9(19): 2413.

[22] Wu G, Chen A. Direct growth of F-doped TiO_2 particulate thin films with high photocatalytic activity for environmental applications[J]. Journal of Photochemistry and Photobiology A: Chemistry, 2008, 195: 47-53.

[23] Antunes C S A, Bitti M, Salamone M, et al. Early stages in the TiO_2-photocatalyzed degradation of simple phenolic and non-phenolic lignin model compounds[J]. Journal of Photochemistry and Photobiology A: Chemistry, 2004, 163(3): 453-462.

[24] Ruggiero R, Machado A E H, Castellan A, et al. Photoreactivity of lignin model compounds in the photobleaching of chemical pulps.1. Irradiation of 1-(3,4-dimethoxyphenyl)-2-(3'-methoxyphenoxy) -1,3-dihydroxypropane in the presence of singlet oxygen sensitizer or hydrogen peroxide in basic methanol solution [J]. Journal of Photochemistry and Photobiology A: Chemistry, 1997, 110(1): 91-97.

[25] Chen A, Rogers E, Compton R G. Abrasive stripping voltammetric studies of lignin and lignin model compounds[J]. Electroanalysis, 2010, 22: 1037-1044.

[26] Zhang S G, Lei W, Xia M Z, et al. QSAR study on N-containing corrosion inhibitors: Quantum chemical approach assisted by topological index[J]. Journal of Molecular Structure, 2005, 732(1/3): 173-182.

[27] Lashgari M, Arshadi M R, Parsafar G A. A simple and fast method for comparison of corrosion inhibition powers between pairs of pyridine derivative molecules [J]. Corrosion, 2005, 61(8): 778-783.

[28] Fujishima A, Honda K. Electrochemical photolysis of water at a semiconductor electrode[J]. Nature, 1972, 238(5358): 37-38.

[29] Zlamal M, Macak J M, Schmuki P, et al. Electrochemically assisted photocatalysis on self-organized TiO_2 nanotubes[J]. Electrochemistry Communications, 2007, 9(12): 2822-2826.

[30] Vinodgopal K, Stafford U, Gray K A et al. Electrochemically assisted photocatalysis. 2. The role of oxygen and reaction intermediates in the degradation of 4-chlorophenol on immobilized TiO_2 particulate films [J]. Journal of Physical Chemistry, 1994, 98 (27): 6797-6803.

[31] Schmidt J A, Heitner C. Light-induced yellowing of mechanical and ultra-high-yield pulps. 2. Radical-induced cleavage of etherified gualacylglycero-β-arylether groups is the main degradative pathway[J]. Journal of Wood Chemistry Technology, 1993, 13(3): 309-325.

[32] Al-Ekabi H, Serpone N. Kinetics studies in heterogeneous photocatalysis. 1 Photocatalytic degradation of chlorinated phenols in aerated aqueous solutions over TiO_2 supported on a glass matrix[J]. Journal of Physical Chemistry, 1988, 92(20): 5726-5731.

[33] Matthews R W. Kinetics of photocatalytic oxidation of organic solutes over titanium-dioxide[J]. Journal of Catalysis, 1988, 111(2): 264-272.

[34] Matthews R W. Photooxidation of organic impurities in water using thin-films of titanium-dioxide[J]. Journal of Physical Chemistry, 1987, 91(12): 3328-3333.

[35] Chen D W, Ray A K. Photodegradation kinetics of 4-nitrophenol in TiO_2 suspension[J]. Water Research, 1998, 323(11): 3223-3234.

[36] Bachrach S M. Computational organic chemistry[M]. John Wiley & Sons, 2007.

[37] Tian M, Thind S, Simko M, et al. Quantitative structure-reactivity study of electrochemical oxidation of phenolic compounds at the SnO_2-based electrode[J]. Journal of Physical Chemistry A, 2012, 116: 2927-2934.

[38] Pearson R G. Electronic spectra and chemical reactivity [J]. Journal of the American Chemical Society, 1988, 110(7): 2092-2097.

[39] Szwacki N G, Sadrzadeh A, Yakobson B I. B-80 fullerene: An ab initio prediction of geometry, stability, and electronic structure[J]. Physical Review Letters, 2007, 98(16):166804.

木质素模型化合物在二氧化钛纳米管上光电氧化的动力学研究

Min Tian, Daniel Liba, Aicheng Chen*

(湖首大学化学系, 加拿大 安大略 P7B 5E1)

摘要: 本文用电化学方法制备了二氧化钛纳米管, 并用扫描电子显微镜和 X 衍射对其形貌及组成进行了表征. 进一步研究了木质素的两个模型化合物 1-(3,4-dimethoxyphenoxy)-2-(2-methoxyphenoxy) -1,3-propanediol (DMP) 和 3-hydroxy-1-(3,4-dimethoxyphenoxy)-2-(2-methoxyphenoxy)-1,3-propanone (HDM)在二氧化钛纳米管上的光电氧化. 在 DMP 的光电氧化过程中, 一个新的紫外吸收峰出现在波长 304 nm 处. 虽然中间体的形成速率随着浓度的增加而增加, 却随着温度的增加而减少. 尽管 HDM 和 DMP 在结构上有很小的差别, 在氧化过程中 DMP 却呈现出很小的吸光度变化, 表明 HDM 不易被光电氧化. 量子化学计算结果也表明,DMP 更容易被氧化, 这个结果与光电氧化的结果相吻合.

关键词: 光电氧化; 二氧化钛纳米管; 原位紫外可见光谱; 木质素模型化合物; DFT 计算